Available online at www.sciencedirect.com
ScienceDirect
Journal of Colloid and Interface Science 302 (2006) 597–604
JOURNAL OF Colloid and Interface Science
www.elsevier.com/locate/jcis

# Electrical conductance study of $\theta$-liquid bridges

Sotiris P. Evgenidis, Margaritis Kostoglou, Thodoris D. Karapantsios *

*Division of Chemical Technology, Department of Chemistry, Aristotle University of Thessaloniki, P.O. Box 116, 54124 Thessaloniki, Greece*

Received 4 May 2006; accepted 24 June 2006

Available online 29 June 2006

**Abstract**

This work investigates the behavior of small liquid bridges that are formed between two horizontal supporting surfaces, aligned at the vertical direction. The contact lines of the liquid bridges are not edge-pinned but free to move across the supporting surfaces with the contact angle as a parameter ($\theta$-bridges). An a.c. electrical conductance technique coupled with high resolution optical images is used to characterize the geometrical details of constant volume liquid bridges when their length is increased gradually until rupture. A mathematical framework is developed for the identification of the geometrical characteristics of $\theta$-liquid bridges explicitly from conductance data. Theoretical predictions show good agreement with measurements for most of the bridge lengths (separation distance between supports) except close to the rupture point where the bridge is highly stretched. It is further shown that for short and moderate separation distances the present model can be used with confidence to determine the bridge volume and neck radius from the electrical signal.


*Keywords:* Liquid bridge; Electrical conductance; Contact angle

## 1. Introduction

The study of liquid bridges between solid surfaces has been the subject of extensive research due to the large number of applications in which liquid bridges are encountered. Some traditional examples are the study of the distribution of phases in porous media with respect to oil recovery applications, capillary evaporation/condensation and binder induced agglomeration of particles which is of importance in operations such as flotation, coating, flocculation and granulation [1–3]. More modern applications are the stability of liquid bridges in flotation zones for producing high quality crystals [4–6], droplet squeezing flow between two plates for studying the dynamics of moving contact lines, e.g., in alignment of matched components during optoelectronics assembly [7,8] the stability of electrically conducting capillary bridges by control of electrostatic stresses [9,10] or even as a means to measure dynamic surface phenomena at short time scales such as wave damping and surfactant squeeze-out from the surface [11].

Traditionally, liquid bridges have been studied either by measuring the force exerted by the liquid bridge to its supporting boundaries or using image processing techniques to identify the liquid bridge profile. In both cases, a usual goal was to estimate surface tension or contact angle from liquid bridge characteristics. However, both techniques require excessive skill and are cumbersome, e.g. [12]. Recently, the apparent electrical conductance of conducting liquid bridges has been suggested as an alternative characteristic parameter from which liquid bridge features can be directly deduced [13,14]. In [13], the conductance of constant volume liquid bridges edge-pinned between two vertical restricted rods ($r$-bridges) was analyzed when their length was varied. In [14], the technique was employed to the case of edge-pinned liquid bridges of reducing volume where slow evaporation was employed as a means to achieve a smooth bridge volume reduction. Here, the conductance technique is extended to the case of constant volume liquid bridges forming between two horizontal plane surfaces to which, however, the contact line of the bridge is not pinned but wetting is controlled by the contact angle as a parameter ($\theta$-bridges). The present tests involve liquid bridges of small volumes, in order to suppress the effect of gravity, that are slowly but gradually stretched until they snap.

* Corresponding author. Fax: +30 2310 99 7759.
*E-mail address:* karapant@chem.auth.gr (T.D. Karapantsios).

0021-9797/$ – see front matter 
doi:10.1016/j.jcis.2006.06.040

The solution of the Young–Laplace equation for the determination of interfacial shape is the subject of many works. An early account is given in [15]. Among the various bridge configurations, considerable attention has been given to the shape of liquid bridges between two spherical particles as a prototype for the study of phenomena in porous media (e.g., evaporation, condensation, oil recovery, etc.). Some typical works concerning the study of the liquid bridge between two spheres are the following: the case of spheres in contact with no gravity influence is examined in [16], the case of zero contact angle is examined in [17] and the stability of the liquid bridge is studied in [18] and [19].

As regards liquid bridges between plane surfaces, Fortes [20] studied them for restricted (rods-so called $r$-bridges) and infinite (with contact angle as parameter-so called $\theta$-bridges) surfaces and for zero Bond number. The study of these liquid bridges in a gravity field was made by Boucher and Evans [21] for restricted surfaces and by Boucher et al. [22] for infinite surfaces. Latter, a stability analysis (somewhat similar to that of Lian et al. [19] for the spheres problem) was given for the restricted surfaces problem and zero gravity by Boucher and Jones [23].

The structure of the work is as follows: First, a theoretical analysis is presented where the computational procedures for the evaluation of the $\theta$-liquid bridge shape and its global apparent conductance value are analyzed. In addition to the exact numerical solution, an approximate analytical solution is also presented. The description of the experimental setup and procedures comes next. Then, theoretical predictions from both solutions are presented and contrasted against each other and against measurements and the results are discussed with regards to advantages for potential applications.

## 2. Theory

### 2.1. Liquid bridge shape

The analysis here will be restricted to the case of liquid bridges which are small enough in order not to have any gravitational influence. In this limit, the shape of the liquid bridge is symmetric with respect to its mid-plane. The no gravity influence can be directly proved by checking the symmetry of the experimental liquid bridge shapes. To facilitate the analysis, a cylindrical coordinate system ($x$ is the axial and $r$ the radial coordinate) will be employed where $x = 0$ is the mid-plane and $r = 0$ is the axis of symmetry, Fig. 1. Only the half space is considered for the calculations. The liquid bridge takes the shape with the less possible surface area exhibiting a contact angle $\theta$ with the substrate. If $V$ is the half volume and $H$ is the half distance between the solid surfaces, the shape $r = Y(x)$ of the liquid bridge is described mathematically by the solution of the equation:

$$\left(1+\left(\frac{\mathrm{d}Y}{\mathrm{d}X}\right)^2\right)^{-3/2}\left[-\frac{\mathrm{d}^2Y}{\mathrm{d}X^2}+\frac{1}{X}\left(1+\left(\frac{\mathrm{d}Y}{\mathrm{d}X}\right)^2\right)\right]=\frac{\Delta P}{\gamma}, \quad (1)$$

where $\gamma$ is the surface tension and $\Delta P$ is the pressure difference between the liquid and the air. The above equation is of second order so it requires two boundary conditions to be solved. In addition a third condition is required since the value of $\Delta P$ is unknown. The three conditions are:

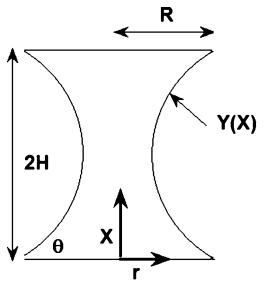


Fig. 1. Geometry of the liquid bridge.

$$\left(\frac{\mathrm{d}Y}{\mathrm{d}X}\right)_{X=H}=\tan(\theta), \quad (2a)$$

$$\left(\frac{\mathrm{d}Y}{\mathrm{d}X}\right)_{X=0}=0, \quad (2b)$$

$$V=\pi\int_0^H Y^2(X)\,\mathrm{d}X. \quad (2c)$$

The above problem is usually solved using direct discretization methods (i.e., finite elements) or transformation to a system of ODE's with the arc length of the liquid bridge as the independent variable [13,14]. In both cases, convergence problems are encountered due to the excessive parameter sensitivity. It is advantageous to exploit the analytical reduction of the complexity of the problem which is feasible for the no-gravity case examined in the present work. The problem treated here is the so-called $\theta$-bridges problem [20] in which the contact angle $\theta$ is known and the radius $R$ of the foot of the liquid bridge must be found. Unlike to the $r$-bridges problem (fixed $R$), there is no suitable characteristic size to non-dimensionalize the problem so it is better to leave it dimensional. However, for the sake of exploiting the semi-analytical solution the following dimensionless variables are considered: $x = X/R$, $y = Y/R$, $y_e = Y_e/R$ where $Y_e$ is the (minimum) radius of the liquid bridge at its neck ($X = 0$). The value $y_e$ is given from the solution of the following transcendental equation

$$\frac{\pi^{1/3}H}{V^{1/3}}=\frac{\int_{y_e}^1 f(z)(1-f^2(z))^{-1/2}\,\mathrm{d}z}{(\int_{y_e}^1 z^2 f(z)(1-f^2(z))^{-1/2}\,\mathrm{d}z)^{1/3}}, \quad (3)$$

$$f(z)=\frac{y_e}{z}+\frac{(\sin(\theta)-y_e)}{(y_e^2-1)}\left(\frac{y_e^2}{z}-z\right). \quad (4)$$

Having found the value of $y_e$, the radius $R$ is computed as:

$$R=\left(\frac{V}{\pi}\right)^{1/3}\left[\int_{y_e}^1 z^2 f(z)\big(1-f^2(z)\big)^{-1/2}\right]^{-1/3} \quad (5)$$

and the shape of the liquid bridge is then given implicitly as:

$$x=\int_{y_e}^{y} f(z)\big(1-f^2(z)\big)^{-1/2}\,\mathrm{d}z. \quad (6)$$

All the above integrals are computed numerically using the orthogonal rule with 1000 discretization points. The combination of the particular integration rule with this large number of discretization points is necessary due to the singularity of the integrand at $z = y_e$. Conventional integration rules need function evaluations at the edges of the integration interval so they fail. The singularity is amenable to integration but leads to a very slow convergence of the numerical integration algorithm so a large number of discretization intervals (1000 is found to be enough after extensive testing) is needed. Equation (3) is solved for $y_e$ using the Newton–Raphson method with numerically computed derivatives. But the convergence depends on the initial value for $y_e$. Before presenting the strategy followed here, a discussion will be given about the multiplicity and stability of the solutions of Eq. (3) (i.e., liquid bridge shapes). First of all, there are the so-called ondulated liquid bridge shapes (non-monotonic in $[0, H]$) which fulfill Eq. (1) but are unstable (not realizable in practice). In addition, there are always two non-ondulated solutions from which only the one with larger $Y_e$ for $\theta < \pi/2$ (smaller $Y_e$ for $\theta > \pi/2$) is stable. For particular $V$ and $\theta$ values the curves $Y_e(H)$ exhibit a bifurcation point where the two solution branches intersect. As $H$ increases $Y_e$ decreases but only up to the bifurcation point where the bridge breaks. All this knowledge is incorporated to a procedure to find $Y_e$ and the corresponding stable liquid bridge evolution as the distance $H$ increases from a small value to the largest one (rupture point). For a particular pair of values of $V$, $\theta$ and starting from an $H$ value such that $H/V^{1/3} < 0.5$, the initial value $y_e = 0.99$ leads always to convergence. Then $H$ increases progressively and a zero order continuation procedure is used, i.e. the solution $y_e$ for a value of $H$ is used as the initial value for the next one. Alternatively, one can avoid the Newton–Raphson step by explicitly computing the $H(y_e)$ curve but it is preferable to trace the evolution of the experimentally controllable parameter $H$. Failure of the convergence means that the break-up distance has been approached. Unfortunately, the break-up distance cannot be computed with arbitrary accuracy due to the finite resolution of $H$ increments and the fact that the Newton–Raphson method fails close to the bifurcation point. The break-up point can be found with arbitrary accuracy by employing the fact that the value of $y_e$ at this point must fulfill the condition:

$$\frac{\mathrm{d}}{\mathrm{d}y_e}\left(\frac{H}{V^{1/3}}\right) = 0. \tag{7}$$

The above equation is solved for $y_e$ by combining a numerical approximation of the derivative with a root bracketing method (Brent method [24]) for the algebraic equation to ensure convergence. Having found the critical $y_e$ value, the break-up distance $H_{crit}$ is found from Eqs. (3), (2c) and (6). The quantity $H_{crit}/V^{1/3}$ depends only on the contact angle $\theta$. This relationship which was shown graphically in [20] can be fitted by the following polynomial form:

$$\frac{H_{crit}}{V^{1/3}} = 0.62905 + 0.065911\left(\frac{2\theta}{\pi}\right) + 1.7885\left(\frac{2\theta}{\pi}\right)^2 - 2.624\left(\frac{2\theta}{\pi}\right)^3 + 1.5664\left(\frac{2\theta}{\pi}\right)^4. \tag{8}$$

### 2.2. Electrical conductance problem

If an electrical potential difference exists between the two supporting rods, the potential distribution in the liquid bridge is given by the solution of the following Laplace equation

$$\frac{1}{r}\frac{\partial}{\partial r}r\frac{\partial P}{\partial r} + \frac{\partial^2 P}{\partial X^2} = 0 \quad \text{in} \quad 0 < r < Y(X) \quad \text{and} \quad 0 < X < H, \tag{9}$$

where $P$ is the normalized electrical potential. The boundary conditions for the above equation are

$$P = 1, \quad \text{for} \quad X = H \quad \text{and} \quad 0 < r < R, \tag{10a}$$

$$P = 0, \quad \text{for} \quad X = 0 \quad \text{and} \quad 0 < r < R, \tag{10b}$$

$$\left(\frac{\partial P}{\partial \vec{n}}\right)_{r=Y(X)} = 0, \tag{10c}$$

where $\vec{n}$ is the unit normal vector. Since there is not a proper reference value for length in this problem, the following apparent conductance (having length units) is defined:

$$K_{app} = \frac{2I}{\pi\kappa\Delta P}, \tag{11}$$

where $I$ is the measured current, $\Delta P$ is the experimental voltage and $\kappa$ the specific conductivity of the liquid.

Having found the potential field $P(x, r)$, the apparent conductance can be computed as

$$K_{app} = 2\int_0^R r\left(\frac{\partial P}{\partial X}\right)_{X=H}\mathrm{d}r. \tag{12}$$

A very crude discretization scheme is used for the solution of the Laplace equation. The domain with dimensions $H \times R$ is discretized uniformly using a basic discretization length $h$ such that $H/h$ is an integer number $M$. Then the shape of the liquid bridge is discretized by computing

$$J_{max}(i) = \mathrm{int}\left(\frac{Y((i-1/2)h)}{h} + \frac{1}{2}\right), \quad i = 1, 2, 3, \ldots, M.$$

The points with coordinates $(ih, jh)$ with $j \leqslant J_{max}$ are assumed to be located in the liquid bridge and the corresponding value of potential is denoted as $P_{i,j}$. The discretized Laplacian equation (second order central finite difference scheme) for the value $P_{i,j}$ in terms of fluxes between adjacent cells is written as ($i = 1, 2, \ldots, M-1$, $j = 1, 2, \ldots, J_{max}$):

$$\left[\left(1 + \frac{1}{2j}\right)P_{i,j+1} - P_{i,j}\right] + \left[\left(1 - \frac{1}{2j}\right)P_{i,j-1} - P_{i,j}\right] + [P_{i+1,j} - P_{i,j}] + [P_{i-1,j} - P_{i,j}] = 0. \tag{13}$$

In case of an adjacent cell being out of the bridge or on the symmetry axis the corresponding terms in the above equation must be neglected. By employing the discretized boundary conditions $P_{0,j} = 0$, $P_{M,j} = 1$ the system of linear equation (13) is solved using the Gauss–Seidel iterative method [25]. After the convergence of the method has been achieved, $K_{app}$ is computed from Eq. (12) by employing the trapezoidal rule for the discretization of the integral and the one side second order finite

difference scheme for the numerical differentiation. The above algorithm although is based to a very crude approximation of the shape of the liquid bridge, can give the $K_{app}$ value with arbitrarily large accuracy provided that the grid is dense enough. For the liquid bridge shapes considered in the present study it is found that $M = 50$ is enough for three digits accuracy. In addition, the algorithm is easily automated and can be incorporated to the code for the evolution of the liquid bridge shape as $H$ increases. So, as the curve $Y_e(d)$ is computed the Laplace equation is solved for each liquid bridge shape in order to determine $K_{app}$. The convergence of the Gauss–Seidel method is accelerated by starting the iterations with the $P_{i,j}$ values found for the previous $H$ value.

### 2.3. Approximate closed form solution of conductance

The simplest possible approximation of the liquid bridge shape is that of a parabola symmetric with respect to plane $x = 0$, i.e., $Y = Y_e + bX^2$ (i.e., the condition (2b) is automatically fulfilled). The coefficients $b$ and $Y_e$ can be found directly by applying the conditions (2a) and (2c) which means that the approximate shape is taken directly from the boundary conditions without employing the governing Eq. (1). From the condition (2a) it is found that $b = \tan(\theta)/2H$. Substitution in Eq. (2c) leads to the following quadratic equation for $Y_e$:

$$Y_e^2 + \frac{H\tan(\theta)}{3}Y_e + \frac{H^2\tan^2(\theta)}{20} - \frac{V}{\pi H} = 0. \tag{14}$$

It is interesting that the structure of the original problem is retained, i.e. there are two solutions for each pair $V$, $\theta$. The practically realizable solution is the one with the larger value of $Y_e$ which can be computed as:

$$2Y_e = -\frac{H\tan(\theta)}{3} + \left(-\frac{4H^2\tan^2(\theta)}{45} + \frac{4V}{\pi H}\right)^{1/2}. \tag{15}$$

The bifurcation point (breaking distance $H_{crit}$) can be found in principle by setting the quantity in parenthesis equal to zero.

An approximate solution of the conductance problem for a slightly deformed cylindrical object connecting two infinite reservoirs is well known in the heat transfer literature [26]. This solution has been extended using the singular perturbation expansion technique [14] to admit larger surface deformations. For the particular case at hand the final result for the conductance is:

$$K_{app} = I_1^{-1}\left(1 - \frac{I_2}{2I_1}\right), \tag{16}$$

where

$$I_1 = \int_0^H \frac{1}{Y^2(X)}\,dX, \tag{17}$$

$$I_2 = \int_0^H \frac{1}{Y^2(X)}\left(\frac{dY}{dX}\right)^2 dX. \tag{18}$$

Considering the approximate parabolic shape for the liquid bridge the above integrations can be performed analytically to give:

$$I_1 = \frac{4H^2}{\tan^2(\theta)}\left[\frac{H}{2c^2(H^2+c^2)} + \frac{1}{2c^3}\arctan\left(\frac{H}{c}\right)\right], \tag{19}$$

$$I_2 = 4\left[-\frac{H}{2(H^2+c^2)} + \frac{1}{2c}\arctan\left(\frac{H}{c}\right)\right], \tag{20}$$

where

$$c = \frac{2Y_eH}{\tan(\theta)}.$$

In is noteworthy that an approximate closed form solution was found for a problem involving the solution of a partial differential equation in a domain defined by an ordinary differential equation.

## 3. Experimental setup and procedures

The experimental setup, Fig. 2, is the same with the one used in [13,14], so only some essential elements are presented here. Liquid bridges are formed between the tips of two equal diameter solid rods which are aligned vertically. The upper rod is coupled with a rotating precision cathetometer with a resolution of 5 μm/division whereas the lower rod is permanently fixed underneath the upper rod. Rods are constructed of stainless steel with a diameter of 8 mm. The cathetometer with the liquid bridge is placed inside a temperature/humidity regulated chamber to prevent evaporation. In this work, temperature is regulated at $25 \pm 1$ °C and relative humidity to $95 \pm 2\%$.

The liquid used in this work is deaerated tap water, filtered mechanically to remove suspended particles larger than 2 μm. The specific conductivity of the water is 760 μS/cm and its surface tension $64 \pm 0.3$ mN/m, at 25 °C. An ultra-precision microsyringe is used to deposit the fluid that forms the liquid bridges with an error in liquid volume determination 1% at most. Experiments are conducted with small bridge volumes—1.1, 1.66, 3 and 4 μl—selected such as to produce a satisfactory span of electrical responses but also diminish gravity effects.

Each experiment starts with setting the separation distance between the rods and forming a liquid bridge of precisely known volume with approximately cylindrical shape. The precise initial shape of the liquid bridge is not a matter of concern

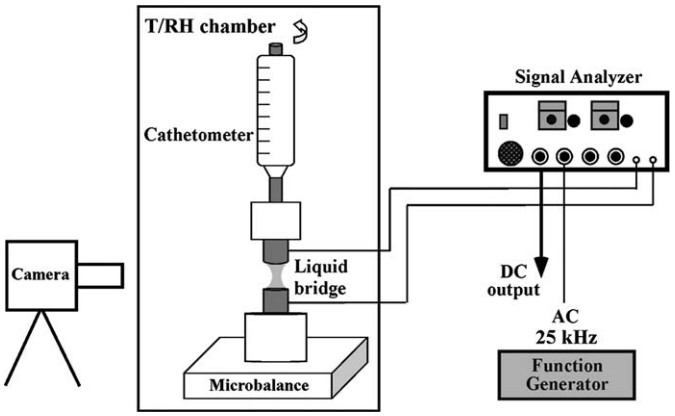


Fig. 2. Schematic diagram of the experimental setup.

since the data reduction analysis takes care of it. In all our experiments $\theta$-liquid bridges are considered, that is, the liquid wets the solid surface at the center of the rods, far away from the circular edges. The separation of the bridge is increased slowly, first in linear steps of 150 or 100 μm, this being followed by gradually smaller steps down to 5 μm at the vicinity of bridge rupture. The initial large displacement steps of the upper rod ascertain good spreading of the liquid on the rods, being several times the full revolution of the cathetometer (50 μm). At each separation distance between the supporting rods, a high resolution picture of the bridge is taken (Canon EOS 350D, 8 Mpixels; EF 100 mm, f/2.8 Macro USM) and stored for later processing.

During the meniscus displacement, the apparent electrical conductance of the bridge is recorded. The conductance probe comprises of the two metallic rods serving as electrodes. Electrical connection of the rotating upper rod is achieved by good contact with a flexible metal strip. The lower rod is connected through an attached lead wire. An a.c. carrier voltage of 0.5 V (peak-to-peak) is applied across the probe at a frequency of 25 kHz in order to suppress undesirable electrode polarization and capacitive impedance. The response of the probe is fed to a special analyzer-demodulator. The analog d.c. voltage output of the analyzer is converted to equivalent conductance $K_{app}$ of the liquid between the electrodes using a calibration curve based on precision resistors. Three records are acquired at all experimental conditions and the reproducibility is good. Pearson correlation coefficients among sampled curves are always above 0.98 whereas average instantaneous signal deviations are around 3%.

## 4. Results and discussion

### 4.1. Theoretical results

Fig. 3 displays the predicted shape of the liquid bridge at various separation distances between the rods, for a liquid bridge volume of 4 μl ($V = 2$ μl). Curves represent a silhouette of one quarter of the bridge, e.g. section inside the dotted line in the inset (full bridge) plot. Due to the $x$ and $r$ symmetry, only one quarter of the bridge is shown. In the calculations, the contact angle is assumed constant and equal to 50°, a value close to experimental observations at long separation distances (see below). What is interesting in this plot is the change in the length of the foot (contact) radius—vertical lines—as the separation distance increases. At the beginning, as $H$ increases the contact radius retracts towards a minimum value which once reached remains constant for an appreciable range of $H$ (curves for other intermediate values of $H$ are not presented for clarity). However, as the bridge stretches further and approaches its rupture point the contact line starts slightly to rise again (curve at largest separation distance). So, in effect, $\theta$-liquid bridges do not have a constant contact radius when their length is altered, at least in cases where their contact angle remains constant (i.e., when the liquid does not anchor at surface imperfections as the contact line moves).

Figs. 4a and 4b show the variation of the electrical conductance predicted for bridges of $V = 2$ and 1 μl, respectively, for various separation distances between the rods, $H$, and for various contact angles. The curves extending up to the end of the horizontal axis are the ones describing the cylindrical bridge configuration ($\theta = 90°$) and are calculated analytically ($K_{app} = V/(\pi H^2)$). A very significant observation in these figures is that for small separation distances, all curves almost coincide irrespective of the contact angle. Hence, at these distances it is the volume of the bridge and not the contact angle that governs the electrical signal; the conductance signal is insensitive to contact angle. As the separation distance increases approaching the rupture point, the curves diverge from each

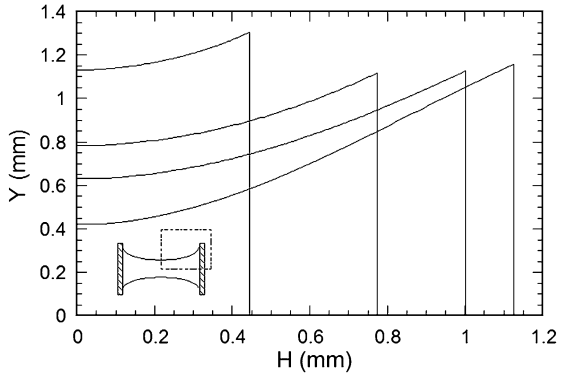


Fig. 3. Liquid bridge shape evolution ($V = 2$ μl, $\theta = 50°$). Curves represent a silhouette of one quarter of the bridge, e.g. section inside the dotted line in the inset (full bridge) plot.

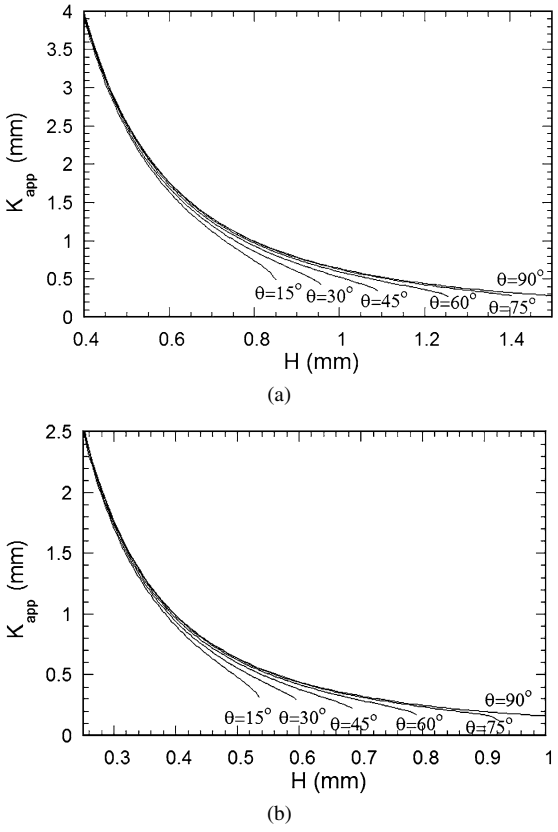


Fig. 4. (a) Apparent conductance for $V = 2$ μl bridge. (b) Apparent conductance for $V = 0.5$ μl bridge.

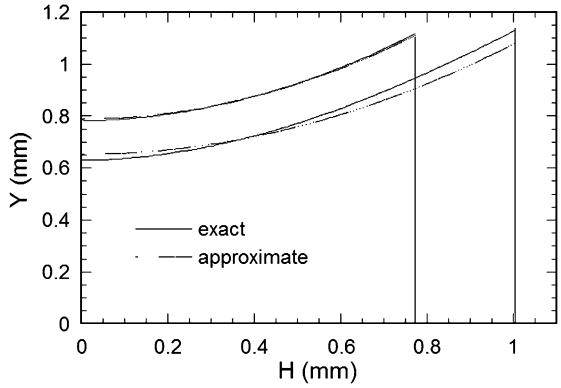


Fig. 5. Exact vs approximate liquid bridge shapes for $V = 2$ μl and $\theta = 50°$.

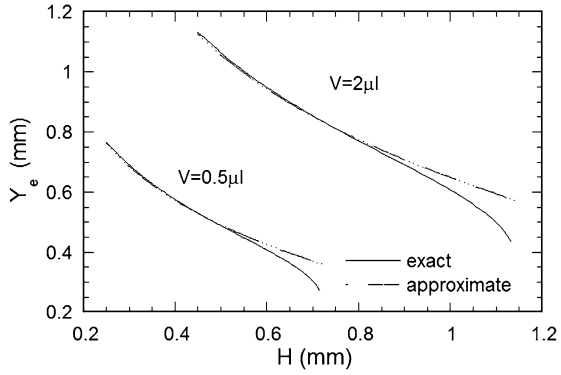


Fig. 6. Exact vs approximate values of neck radius for $V = 0.5$ and 2 μl and $\theta = 50°$.

other. This implies that contact angles may be deduced from electrical measurements only when using $H$ values close to bridge rupture. It is noted that the smaller the contact angle, the shorter the separation distance for rupture to occur. On the other hand, as $\theta$ increases the conductance at the rupture point first decreases, e.g., from $\theta = 15°$ to 60°, and then increases from $\theta = 60°$ to 90°. This chiefly reflects the variation of the radius of the bridge neck at the rupture point.

Before comparing measurements with predictions it is useful to show what is the limit of applicability of the approximate analytical solution derived in the theory section. Fig. 5 shows the shape of a bridge calculated by the exact and the approximate solutions for two separation distances between the rods ($V = 1$ μl and $\theta = 50°$). It is apparent that differences become noticeable only at large distances. Fig. 6 displays the variation of the bridge neck radius, $Y_e$, with respect to $H$ for two bridges of different volume ($V = 0.5$ and 2 μl) but the same contact angle ($\theta = 50°$). Once again, it is seen that at the initial stages of bridge extension the approximate solution produces acceptable results. When $H$ increases beyond ∼50% of the total distance until rupture, there is a progressively increasing divergence between the exact and approximate solutions which, in fact, excludes the latter from meaningful comparisons with experimental data. The accuracy of the singular perturbation approximation, Eq. (16), for the conductance also decreases as the distance increases but at a slower rate than the accuracy of the shape approximation of the bridge. This means that under conditions of validity of the quadratic approximation for the shape

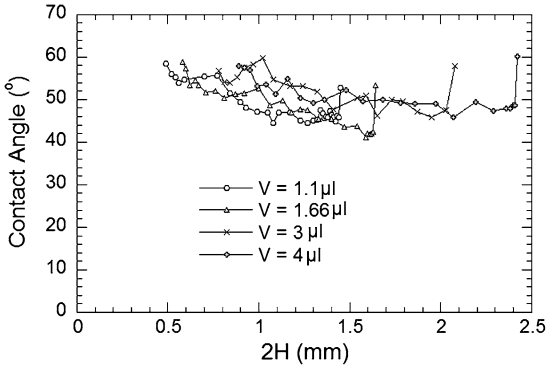


Fig. 7. Experimental contact angles vs liquid bridge length for $V = 1.1$, 1.66, 3 and 4 μl bridges.

(see Fig. 6) Eqs. (16), (19) and (20) can be used for the computation of the conductance of the liquid bridge.

### 4.2. Experimental results and comparisons with predictions

The experimentally determined contact angles are presented in Fig. 7. These values are averages of the four angles determined at the corners of every bridge image (two at the top and two at the bottom). Despite the fluctuations in the measured values—due to local inhomogeneities at the surface of the supporting rods—it is apparent that the contact angle is not constant during bridge deformation. It declines from initially around 60° to values below 50° and in one case ($V = 0.83$ μl) even down to 40°. One may note that for the employed system, the contact angle at long separation distances is roughly $45° \pm 5°$. After bridge rupture, the equilibrium contact angle (last point of each data series) rises again to values above 50°, even close to 60° for the larger bridges. Thus, despite the employed slow rate of bridge deformation in the experiments, the contact angle does not take its equilibrium value but shifts towards smaller values (the receding contact angle value for the highly wettable stainless steel surface is ∼10° [27]).

Both the effects of fluctuations and shift in contact angle cast doubt on the possibility to derive the value of the contact angle from the electrical response of the bridge since this value depends on local surface inhomogeneities and the deformation history of the bridge. Nevertheless, for short bridges (far from their rupture point), where the value of the contact angle is irrelevant, the electrical signal is shown below to be a very sensitive indicator of bridge volume; much better than optical means.

Fig. 8 compares the variation of the experimentally measured neck radius of the employed liquid bridges with theoretical predictions based on the exact solution of the descriptive equations. For the calculations, the contact angle is assumed constant at the value measured close to the rupture point. On the whole, the agreement between theoretical and experimental results is good. However, the theory fails to predict the behavior a little prior to rupture. In all cases, the experimental bridges extend a bit further than predicted by the theory before becoming unstable and snap. It seems that the present model does not describe satisfactory the phenomena occurring at maximum bridge stretching where the bridge shape is highly distorted and

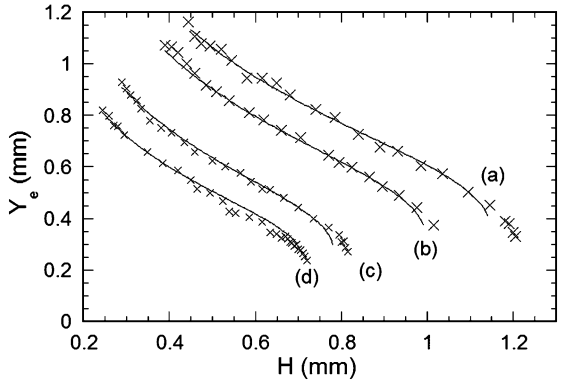


Fig. 8. Theoretical vs experimental values of neck radius: (a) $V = 2$ μl, $\theta = 50°$, (b) $V = 1.5$ μl, $\theta = 45°$, (c) $V = 0.83$ μl, $\theta = 40°$, (d) $V = 0.55$ μl, $\theta = 45°$.

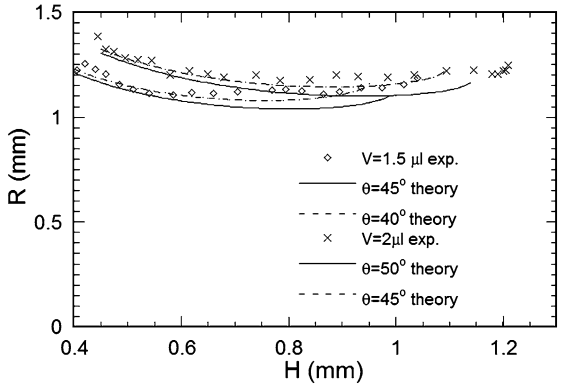


Fig. 9. Contact (foot) radius theoretical vs experimental for $V = 2$ and 1.5 μl, respectively.

further work is required in that direction. It appears that there is yet another stabilizing mechanism for the bridge which is not taken into account in the theory. Gravity may play a small role for distances close to the rupture point but in general its effect is expected in the opposite direction (destabilization of the bridge) [13]. There is a possibility that the additional stabilization may originate from a distribution of contact angles along the contact line, evidence of which, however, cannot be inferred from the 2D images acquired in this work. At small bridge stretching the conformity with the experiment is adequate for data reduction purposes which, however, is a region of low sensitivity of conductance to changes of contact angle (Figs. 4a and 4b).

Fig. 9 shows the experimentally determined contact (foot) radius, $R$, of two liquid bridges as a function of the bridge length, $H$, along with the corresponding theoretical predictions. For each bridge, calculations are performed with two values of the contact angle in order to demonstrate the sensitivity of contact radius with respect to contact angle. As already mentioned in Fig. 3, the contact radius decreases first and then increases with bridge length. This can be seen in both experiments and predictions. Moreover, there is a trade-off between contact radius and rupture length when varying theoretically the contact angle, the effect of contact angle being more profound as the bridge approaches its rupture point. Higher contact angles yield rupture lengths closer to experimental observations but predict

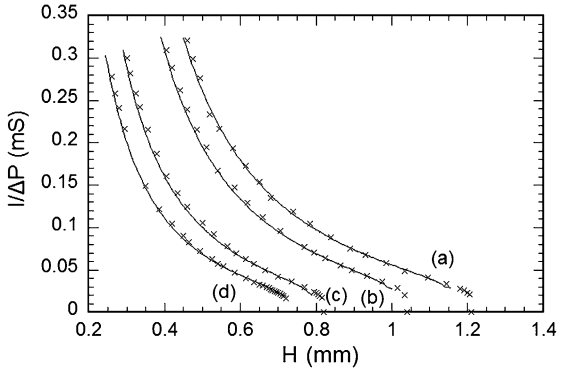


Fig. 10. Theoretical vs experimental electrical conductance ($I/\Delta P$) with respect to liquid bridge length for: (a) $V = 4$ μl, $\theta = 50°$, (b) $V = 3$ μl, $\theta = 45°$, (c) $V = 1.66$ μl, $\theta = 40°$, (d) $V = 1.1$ μl, $\theta = 45°$.

smaller contact radius than experimentally determined and vice versa. Again, the present model seems not to describe adequately what occurs near the rupture point. It is very interesting that unlike the intuitively expected picture of a contact line slipping on the rod when the bridge is stretched beyond a certain degree—in an effort to retain the contact angle constant [14,28,29]—here it is shown, both theoretically and experimentally, that a liquid bridge can be stretched until rupture with its contact angle and contact radius (wetted area) lying within a narrow range.

Fig. 10 presents recorded electrical conductance time records for different liquid bridge volumes against theoretical predictions. The theoretical value of $I/\Delta P$ is computed from Eq. (11). Despite the difference in bridge volume, qualitatively comparable curves are obtained. All traces display a monotonous decay with separation distance being steeper at smaller separation distances and more gradual at larger ones. At the vicinity of bridge rupture all curves are characterized by an abrupt drop of the signal which, as already mentioned, cannot be described by the model.

It is evident from Fig. 10 that the response of the electrical technique is very sensitive to bridge volume and length and so it may be used for the determination of either one of these parameters if the other is known. Considering that this is an easy macroscopic measurement then the advantage over the cumbersome optical measurement is apparent. Comparing Figs. 8 and 10 at the vicinity of bridge rupture reveals that electrical measurement is a very sensitive indicator of neck radius since a small change in neck radius corresponds to a larger change (on a percentage basis) in electrical signal. The latter can be extremely useful in measuring film thinning and rupture of the liquid layer between two surfaces, e.g. bubbles, that approach or move closely past each other. Such phenomena are encountered in foam production, flotation, etc.

## 5. Conclusions

In the present work an electrical conductance technique is explored as a means to study the configuration of $\theta$-liquid bridges (those forming between infinite surfaces). A mathematical framework is developed which allows the computation of

the liquid bridge shape at different lengths when the bridge volume is known or vice versa. The electrical conductance of the liquid bridge is computed through the solution of the Laplace equation in axisymmetric geometry. An approximate analytical solution is also provided giving accurate results for the less distorted bridges (away from their rupture point). Several experiments are performed in which the conductance of constant volume liquid bridges is measured at different separation distances between the supporting rods. By matching the theoretical with experimental curves several features of the bridges can be estimated with confidence, e.g., volume, length, contact (foot) radius, neck radius. However, the technique is not so accurate for the determination of the contact angle of the bridge on the rods since this determination depends not only on a number of experimental parameters (local surface inhomogeneities of the rods, deformation history of the bridge, etc.) but also on the low sensitivity of electrical conductance with respect to contact angle in regions far from the rupture point. Regarding potential practical applications, it seems interesting to employ this technique to examine the influence of surfactant systems on the shape and morphology of conducting liquid bridges like those encountered in tertiary oil recovery. In addition, it may be used for studying film thinning phenomena between approaching bubbles in systems encountered in foam production, flotation processes, etc.

## References

[1] S.J.R. Simons, R.J. Fairbrother, Powder Technol. 110 (2000) 44.
[2] C.D. Willett, M.J. Adams, S.A. Johnson, J.P.K. Seville, Langmuir 16 (2000) 9396.
[3] Y.I. Rabinovich, M.S. Esayanur, B.M. Moudgil, Langmuir 21 (2005) 10992.
[4] V. Luengo, J. Meseguer, I.E. Parra, Exp. Fluids 34 (2003) 412.
[5] M. Sakurai, N. Ohishi, A. Hirata, Acta Astronautica 55 (2004) 977.
[6] D.E. Melnikov, V.M. Shevtsova, J.C. Legros, Acta Astronautica 56 (2005) 601.
[7] S.N. Reznik, A.L. Yarin, Int. J. Multiphase Flow 28 (2002) 911.
[8] K.F. Harsh, V.M. Bright, Y.C. Lee, Sens. Actuators A 77 (1999) 237.
[9] D.B. Thiessen, M.J. Marr-Lyon, P.L. Marston, J. Fluid Mech. 457 (2002) 285.
[10] M.J. Marr-Lyon, D.B. Thiessen, F.J. Blonigen, P.L. Marston, Phys. Fluids 12 (5) (2000) 986.
[11] N.M. Patel, P.L. Taylor, M.R. Fisch, C. Rosenblatt, Colloids Surf. A 218 (2003) 65.
[12] E. Wolfram, J. Pinder, Acta Chem. Acad. Sci. Hung. 100 (1979) 433.
[13] M. Kostoglou, T.D. Karapantsios, J. Colloid Interface Sci. 227 (2000) 282.
[14] T.D. Karapantsios, M. Kostoglou, J. Colloid Interface Sci. 255 (2002) 177.
[15] J.F. Padday, Pure Appl. Chem. 48 (1976) 485.
[16] J.C. Melrose, AIChE J. 12 (1966) 986.
[17] M.A. Erle, D.C. Dyson, N.R. Morrow, AIChE J. 17 (1971) 115.
[18] D.N. Mazzone, G.I. Tardos, R. Pfeffer, J. Colloid Interface Sci. 113 (1986) 544.
[19] G. Lian, C. Thornton, M.J. Adams, J. Colloid Interface Sci. 161 (1993) 138.
[20] M.A. Fortes, J. Colloid Interface Sci. 88 (1982) 338.
[21] E.A. Boucher, M.J.B. Evans, J. Colloid Interface Sci. 75 (1980) 409.
[22] E.A. Boucher, M.J.B. Evans, S. McGarry, J. Colloid Interface Sci. 89 (1982) 154.
[23] E.A. Boucher, T.G.J. Jones, J. Colloid Interface Sci. 126 (1988) 469.
[24] W.H. Press, S.A. Teukolsky, W.T. Vetterling, B.P. Flannery, in: Numerical Recipes. The Art of Scientific Computing, Cambridge Univ. Press, New York, 1992.
[25] M.N. Özisik, in: Boundary Value Problems of Heat Conduction, International Textbook Company, Scranton, 1968.
[26] M.D. Michailov, M.N. Özisik, in: Unified Analysis and Solutions of Heat and Mass Diffusion, Wiley, New York, 1984, p. 132.
[27] S. Chandra, M. di Marzo, Y.M. Qiao, P. Tartarini, Fire Safety J. 27 (1996) 141.
[28] X. Pepin, D. Rosseti, S.M. Iveson, S.J.R. Simons, J. Colloid Interface Sci. 232 (2000) 289.
[29] X. Pepin, D. Rosseti, S.J.R. Simons, J. Colloid Interface Sci. 232 (2000) 298.